Advantages in angiogenesis imaging: Hsu and Chen review the current state of anatomic, functional, and molecular imaging of angiogenesis, an intensely studied area of cancer research that holds great promise. *Page 511*

Correlative imaging in hypoxia and angiogenesis: Langen and Eschmann provide an introduction to current imaging approaches in hypoxia and angiogenesis and preview an article on these topics in this issue of *JNM*. *Page 515*

^{18}F-FDG and tumor perfusion: Mullani and colleagues investigate whether early, first-pass ^{18}F-FDG PET can be used to estimate regional blood flow in tumors, a technique with promise for facilities that lack cyclotrons for ^{15}O-water production. *Page 517*

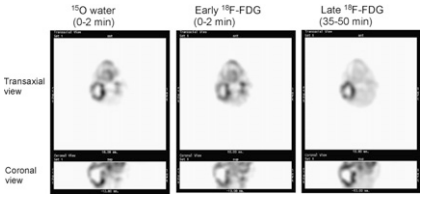

Preoperative imaging in thyroid carcinoma: Koopmans and colleagues explore optimal imaging approaches (including ^{18}F-DOPA PET, ^{18}F-FDG PET, scintigraphic, CT, and MR imaging) in presurgical tumor localization in patients with recurrent medullary thyroid cancer. *Page 524*

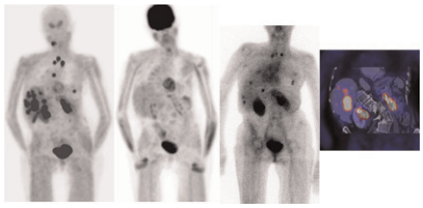

PET/CT in posttherapy HNSCC: Ong and colleagues assess the predictive utility of ^{18}F-FDG PET/CT in patients with locoregional advanced head and neck squamous cell carcinoma after concurrent chemotherapy and radiation therapy. *Page 532*

Scintigraphy and brachytherapy seeds: Kono and colleagues describe the use of a novel scintigraphic method for monitoring localization and migration of implanted ^{125}I seeds after permanent brachytherapy for prostate cancer. *Page 541*

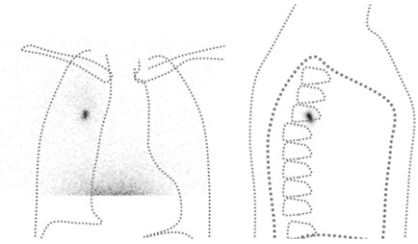

Prevention of ^{131}I-induced sialadenitis: Silberstein reports on a study designed to determine whether administration of pilocarpine can reduce the salivary symptoms of pain and xerostomia caused by ^{131}I therapy for papillary and follicular thyroid carcinoma. *Page 546*

MPS and stent prognosis: Zellweger and colleagues explore the ability of myocardial perfusion scintigraphy to predict events related to late stent thrombosis and restenosis after percutaneous coronary intervention with drug-eluting stents. *Page 550*

Progenitor cells after coronary recanalization: Kendziorra and colleagues investigate relative changes in human myocardial perfusion and glucose metabolism induced by intracoronary administration of blood-derived circulating progenitor cells after recanalization of total coronary occlusion. *Page 557*

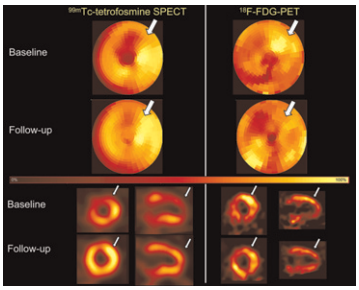

CTA vs. SPECT for stenosis severity: Sato and colleagues compare the clinical value of information from 64-slice CT angiography and stress myocardial perfusion imaging in 104 patients with suspected coronary artery disease. *Page 564*

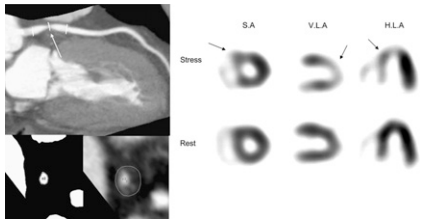

^{18}F-DOPA PET in neuroendocrine tumors: Jager and colleagues provide an educational overview of the radiosynthesis, uptake, and metabolism of ^{18}F-DOPA and its clinical applications in PET imaging of neuroendocrine tumors. *Page 573*

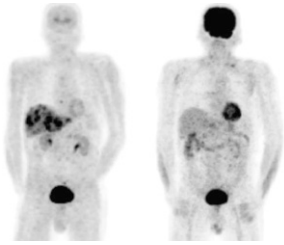

Modeling considerations for ^{11}C-CUMI-101: Milak and colleagues report on studies of optimal modeling parameters for this 5-HT_{1A}R agonist in the baboon and describe its potential applications in PET assessment of the pathophysiology of neuropsychiatric disorders in humans. *Page 587*

Tumor hypoxia and angiogenesis: Picchio and colleagues use digital autoradiography of co-injected ^{18}F-FAZA and a radiolabeled glycosylated RGD-containing peptide to explore spatial correlations between angiogenesis and tissue hypoxia in tumor xenografts. *Page 597*

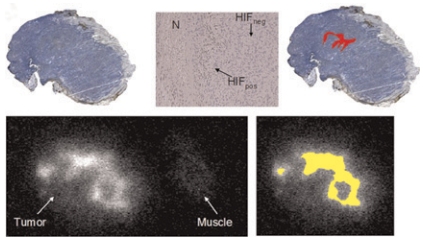

Model-corrected input function for PET: Fang and Muzic describe a method for deriving an input function for small-animal ^{18}F-FDG PET studies from dynamic image data and only one or no blood sample, accounting for both spillover and partial-volume effects. . . . . ***Page 606***

Cancer imaging with ^{11}C-glycylsarcosine PET: Mitsuoka and colleagues report on a novel PET tracer targeted to H^+/peptide transporter(s) and compare its specificity with that of ^{18}F-FDG in distinguishing between tumor and inflammation. . . . . ***Page 615***

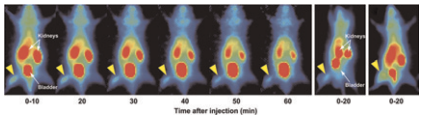

^{111}In-DTPA-folate and pemetrexed: Müller and colleagues investigate the potential for preinjection of an antifolate in improving tumor selectivity and reducing renal uptake of ^{111}In-DTPA-folate in a human ovarian cancer xenografted mouse model. . . . . ***Page 623***

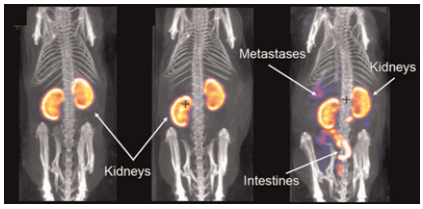

^{18}F-labeled myocardial perfusion tracer: Huisman and colleagues describe the biodistribution and imaging characteristics of a novel ^{18}F-labeled myocardial perfusion agent in a rat model and discuss its potential advantages in clinical PET applications. . . . . ***Page 630***

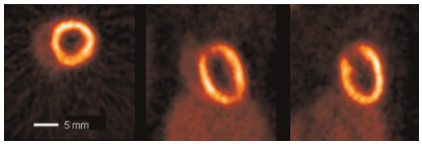

Imaging probes for HSV1-*tk*: Miyagawa and colleagues compare ^{18}F-labeled pyrimidine nucleoside analogs and acycloguanosine analogs using a stable HSV1-*tk* transduced cell line and wild-type RG2 cells to identify an optimal probe for reporter gene imaging. . . . . ***Page 637***

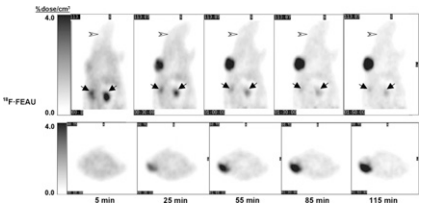

PET at the blood–brain barrier: Zoghbi and colleagues evaluate ^{11}C-loperamide, an opiate receptor agonist, as a PET tracer to measure permeability-glycoprotein function in vivo. . . . . ***Page 649***

PET denoising with MR/CT wavelets: Turkheimer and colleagues demonstrate the use of structural data from matched anatomic images in a multiresolution model to enhance signal-to-noise ratio in PET images. . . . . ***Page 657***

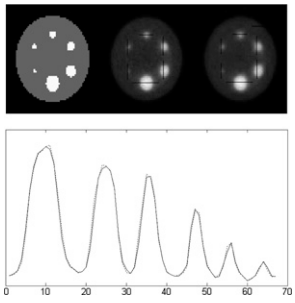

Monitoring VEGFR expression after MI: Rodriguez-Porcel and colleagues report on the development of a PET tracer designed to image vascular endothelial growth factor expression as a measure of left ventricular remodeling after myocardial infarction. . . . . ***Page 667***

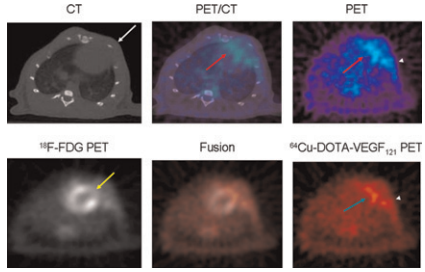

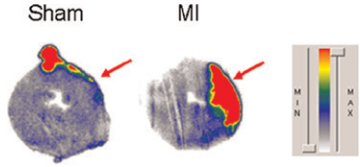

Effects of rituximab: Kapadia and colleagues assess the antiproliferative and possible radiosensitizing capabilities of rituximab, an anti-CD20 monoclonal antibody, and discuss the implications of their results for the design of radioimmunotherapy trials. . . . . ***Page 674***

^{18}F-FDG embryo dosimetry: Zanotti-Fregonara and colleagues provide data on embryo tissue uptake in a case study of a patient who underwent PET/CT for tumor surveillance and was later found to have been pregnant at the time of imaging. . . . . ***Page 679***

ON THE COVER

The peptide PET tracer ^{11}C-glycylsarcosine is a promising tumor-imaging agent and is superior to ^{18}F-FDG for distinguishing between tumors and inflammatory tissue. In mice with tumor in the right hind leg and turpentine-induced inflammation in the left hind leg, the inflammatory tissue showed uptake of ^{18}F-FDG but no specific uptake of ^{11}C-glycylsarcosine. This tracer could be useful for the detection of many types of cancer.

See page 620.